


Five metal imidazole dicarboxylate-based compounds comprising $M_3(\text{MIDC})_2$ entities ($M = \text{Zn}^{2+}, \text{Co}^{2+}, \text{Mn}^{2+}$): syntheses, structures and properties

Jiang-Feng Song, Yang Li, Rui-Sha Zhou, Jia Shao, Lu Wang & Xiao-Bing Cui

To cite this article: Jiang-Feng Song, Yang Li, Rui-Sha Zhou, Jia Shao, Lu Wang & Xiao-Bing Cui (2015) Five metal imidazole dicarboxylate-based compounds comprising $M_3(\text{MIDC})_2$ entities ($M = \text{Zn}^{2+}, \text{Co}^{2+}, \text{Mn}^{2+}$): syntheses, structures and properties, Journal of Coordination Chemistry, 68:20, 3651-3666, DOI: [10.1080/00958972.2015.1071483](https://doi.org/10.1080/00958972.2015.1071483)


To link to this article: <http://dx.doi.org/10.1080/00958972.2015.1071483>

 View supplementary material 

 Accepted author version posted online: 13 Jul 2015.
Published online: 03 Aug 2015.

 Submit your article to this journal 

 Article views: 78

 View related articles 

 View Crossmark data 

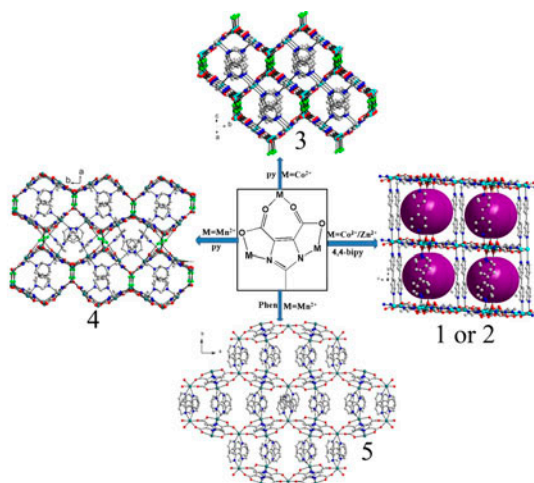
Five metal imidazole dicarboxylate-based compounds comprising $M_3(\text{MIDC})_2$ entities ($M = \text{Zn}^{2+}, \text{Co}^{2+}, \text{Mn}^{2+}$): syntheses, structures and properties

JIANG-FENG SONG^{*†}, YANG LI[†], RUI-SHA ZHOU[†], JIA SHAO[†], LU WANG[†] and XIAO-BING CUI[‡]

[†]Department of Chemistry, North University of China, Taiyuan, PR China

[‡]College of Chemistry and State Key Laboratory of Inorganic Synthesis and Preparative Chemistry, Jilin University, Changchun, PR China

(Received 3 February 2015; accepted 8 June 2015)



Using a method, which can effectively control the coordination mode of H_3MIDC , we constructed a series of new coordination compounds containing honeycomb-like $[\text{M}_3(\text{MIDC})_2]_n$ layers.

Five metal imidazole dicarboxylate-based compounds, $\{[\text{Zn}_3(\text{MIDC})_2(4,4'\text{-bipy})_3](4,4'\text{-bipy}) \cdot 8\text{H}_2\text{O}\}_n$ (**1**), $\{[\text{Co}_3(\text{MIDC})_2(4,4'\text{-bipy})_3](4,4'\text{-bipy}) \cdot 6\text{H}_2\text{O}\}_n$ (**2**), $\{[\text{Co}_3(\text{MIDC})_2(\text{py})_2(\text{H}_2\text{O})_2]\}_n$ (**3**), $\{[\text{Mn}_6(\text{MIDC})_4(\text{py})_5(\text{H}_2\text{O})_4]\}_n$ (**4**), and $\{[\text{Mn}_3(\text{MIDC})_2(\text{Phen})_3(\text{H}_2\text{O})_2]\}_n$ (**5**) (H_3MIDC = 2-methyl-1H-imidazole-4,5-dicarboxylic acid; 4,4'-bipy = 4,4'-bipyridine; py = pyridine; Phen = 1,10-phenanthroline), have been synthesized under hydrothermal conditions and characterized by elemental analyses, IR spectroscopy, thermogravimetric analysis, and single-crystal X-ray diffraction. We control the coordination modes of H_3MIDC via hydrazine and obtained a series of coordination compounds containing honeycomb-like $[\text{M}_3(\text{MIDC})_2]_n$ layers. We also investigated the effects of different neutral terminal or bridging ligands on $[\text{M}_3(\text{MIDC})_2]_n$ layers. Coplanar $[\text{M}_3(\text{MIDC})_2]_n$

*Corresponding author. Email: jfsong0129@nuc.edu.cn

layers and 4,4'-bipy were used to construct 3-D frameworks of **1** and **2**. Puckered $[M_3(\text{MIDC})_2]_n$ layers were found in **3–5**; **4** is the first $[M_3(L)_2]_n$ layer structure with two crests and troughs during each period ($L =$ imidazole-4,5-dicarboxylic acid or its analog). Compound **5** is the first puckered $[M_3(L)_2]_n$ layer structure decorated by chelating neutral ligands. Compound **1** exhibits weak blue photoluminescence in the solid state at room temperature. Variable-temperature magnetic susceptibility measurements of **2–5** indicate strong antiferromagnetic interactions.

Keywords: Coordination polymer; Crystal structure; Imidazole dicarboxylate

1. Introduction

Coordination polymers are rapidly increasing due to diverse topologies and potential applications as functional materials [1–20]. Significant progress has been made on coordination polymers, however, their controllable syntheses still remain a challenge because the self-assembly processes are often influenced by compositional (chemical structures of chosen ligands, coordination geometries of metal ions, pH, solvent, etc.) and process parameters (reaction time, temperature, and pressure) [21–27]. Choice of ligands is one of the most important parameters influencing the formation of coordination polymers with novel topologies and unique properties. Polytypic carboxylates are excellent candidates for constructing architectures because the molecules generally have good ligating ability to different metal ions. The coordination versatility of polytypic carboxylates also leads to a high level of unpredictability in reaction outcomes because each single O-donor can bind one, two, and even three metal ions. So, the effective control of coordination modes of chosen ligands is important for the rational assembly of coordination polymers [19].

Recently, 4,5-imidazole dicarboxylate (H_3IDC) and its analogs have received much attention in the building of coordination polymers due to diversified coordination modes and good ligating abilities; many coordination polymers constructed from IDC^{3-} or its analogs have been reported [28–39]. In these reported complexes, coordination diversities of IDC^{3-} have been discussed, however, the effective control of coordination modes of IDC^{3-} or its analogs is usually neglected. Based on the analysis of reported coordination polymers, we found that IDC^{3-} or its analogs adopt the same tri(chelating)coordination mode to interact with metal centers and assemble into $[M_3(L)_2]$ layers in $[\text{Mn}_6(\text{EIDC})_4(\text{py})_4(\text{H}_2\text{O})_4]_n$ [32], $\{[\text{Zn}_3(\text{IDC})_2(4,4'\text{-bipy})_3](4,4'\text{-bipy})\cdot 8\text{H}_2\text{O}\}_n$ [38], $\{[\text{Co}_3(\text{IDC})_2(4,4'\text{-bipy})_3]\cdot 6\text{H}_2\text{O}\cdot \text{DMF}\}_n$ [39], $\{[\text{Co}_3(\text{IDC})_2(\text{pyz})_3]\cdot 8\text{H}_2\text{O}\}_n$ [40], $\{[\text{Co}_3(\text{IDC})_2(4,4'\text{-bipy})_3]\cdot 4,4'\text{-bipy}\cdot 8\text{H}_2\text{O}\}_n$ [40], $\{[\text{Co}_3(\text{IDC})_2(2,5\text{-bptz})_3]\cdot 2,5\text{-bptz}\cdot 9\text{H}_2\text{O}\}_n$ [40] and $[\text{Zn}_3(\text{MIDC})_2(\text{H}_2\text{O})_2(\text{DMF})_2]_n$ [41] ($\text{H}_3\text{EIDC} = 2\text{-ethyl-1H-imidazole-4,5-dicarboxylic acid}$; $4,4'\text{-bipy} = 4,4'\text{-bipyridine}$; $\text{pyz} = \text{pyrazine}$; $2,5\text{-bptz} = 2,5\text{-bis(pyrid-4-yl)-1,3,4-thiadiazole}$). From a design perspective, two questions have been proposed: (1) how to effectively control the coordination modes of IDC^{3-} or its analogs so as to obtain $[M_3(L)_2]_n$ layers and (2) if the ligating sites at both sides of a $[M_3(L)_2]_n$ layer are occupied by neutral organic ligands, will the 2-D layer be further connected to form a 2-D or 3-D coordination framework. So, control of IDC^{3-} or its analogs to adopt the special coordination mode will be fatal for the rational synthesis of targeted framework structures based on $[M_3(L)_2]_n$ layers.

As part of our ongoing efforts in the design and synthesis of crystalline materials based on the analogs of H_3IDC [41–43], $[\text{Zn}_3(\text{MIDC})_2(\text{H}_2\text{O})_2(\text{DMF})_2]_n$ with $[M_3(\text{MIDC})_2]_n$ layer was synthesized with help of triethylamine [41], however, we found that it is not easy to effectively control the coordination modes of H_3MIDC using triethylamine. Recently, we

developed an effective method that can make 2-ethyl-1H-imidazole-4,5-dicarboxylic acid (H₃EIDC) to adopt the tri(chelating)coordination mode using hydrazine as a deprotonating agent [43]. As continuation of our research and based on the method we developed, H₃MIDC was chosen as an anionic linker to construct a series of new coordination compounds containing [M₃(MIDC)₂]_n layers via control of MIDC³⁻ adopting the special tri(chelating)coordination mode. In this paper, we report five new coordination polymers based on similar [M₃(MIDC)₂]_n layers, {[Zn₃(MIDC)₂(4,4'-bipy)₃](4,4'-bipy)·8H₂O}_n (**1**), {[Co₃(MIDC)₂(4,4'-bipy)₃](4,4'-bipy)·6H₂O}_n (**2**), {[Co₃(MIDC)₂(py)₂(H₂O)₂]_n (**3**), {[Mn₆(MIDC)₄(py)₅(H₂O)₄]_n (**4**), and {[Mn₃(MIDC)₂(Phen)₃(H₂O)₂]_n (**5**). In **1–5**, each MIDC³⁻ coordinates to three metal centers in tri(chelating) coordination mode to form similar honeycomb-like [M₃(MIDC)₂]_n layers in which the ligating sites at both sides were decorated by different neutral terminal or bridging ligands.

2. Experimental

2.1. Materials and measurements

All chemicals and solvents purchased were of reagent grade and used without purification except H₃MIDC. H₃MIDC was prepared according to a reference [44]. Elemental analysis (C, H, N) was performed on a Perkin-Elmer 240C elemental analyzer. IR spectra were measured on a Perkin-Elmer Spectrum One FT-IR spectrometer using KBr pellets. Thermogravimetric analyses (TGA) were performed on a Perkin-Elmer TGA-7000 thermogravimetric analyzer under flowing air at a temperature ramp rate of 10 °C min⁻¹. Photoluminescence (PL) excitation and emission spectra were recorded with a Jobin Yvon Fluoro Max-4 spectrophotometer equipped with a 150 W xenon lamp as the excitation source at room temperature. Variable-temperature magnetic susceptibility measurements were carried out using a SQUID magnetometer MPMS XL-7 (Quantum Design) at 1.0 kOe from 2 to 300 K.

2.1.1. Synthesis of {[Zn₃(MIDC)₂(4,4'-bipy)₃](4,4'-bipy)·8H₂O}_n (1**).** A solution of H₃MIDC (17.0 mg, 0.1 mmol) in 6 mL water containing NH₂NH₂·H₂O (30 μL, concentration: 50%) was directly mixed with a 1 mL 0.10 mol L⁻³ ZnCl₂ solution at room temperature in a 15 mL beaker. A solution of 4,4'-bipy (7.8 mg, 0.05 mmol) in 2 mL methanol was added to the mixture. The resulting mixture was transferred and sealed in a 25 mL Teflon-lined stainless steel reactor and heated at 170 °C for 72 h. Upon cooling to room temperature, colorless crystals were filtered and washed with ethanol. Yield: 25% (based on H₃MIDC). Elemental Anal. Calcd C₅₂H₅₄N₁₂O₁₈Zn₃ (1299): C, 46.81; H, 4.35; N, 12.60. Found: C, 46.85; H, 4.35; N, 12.59. IR data (KBr, cm⁻¹) (w = weak, m = medium, s = strong): 3378(m), 2932(w), 1579(s), 1419(s), 1253(m), 1128(m), 1066(m), 1005(w), 848(m) 798(m), 694(m), 495(m).

2.1.2. Synthesis of {[Co₃(MIDC)₂(4,4'-bipy)₃](4,4'-bipy)·6H₂O}_n (2**).** The procedure was the same as that for **1** except that ZnCl₂ was replaced by CoCl₂ (0.10 mol L⁻³). Upon cooling to room temperature, red crystals were filtered and washed with ethanol. Yield: 67% (based on H₃MIDC). Elemental Anal. Calcd C₅₂H₅₀Co₃N₁₂O₁₄ (1243): C, 50.20; H, 4.02;

N, 13.52. Found: C, 50.19; H, 4.05; N, 13.49. IR data (KBr, cm^{-1}): 3397(s), 2924(w), 1576(s), 1419(s), 1241(m), 1120(m), 1030(w), 837(m), 692(m).

2.1.3. Synthesis of $\{[\text{Co}_3(\text{MIDC})_2(\text{py})_2(\text{H}_2\text{O})_2]\}_n$ (3**).** The procedure was the same as that for **2** except that 4,4'-bipy was replaced by py (1 mL). Upon cooling to room temperature, red crystals were filtered and washed with ethanol. Yield: 85% (based on H_3MIDC). Elemental Anal. Calcd $\text{C}_{22}\text{H}_{20}\text{Co}_3\text{N}_6\text{O}_{10}$ (705.23): C, 37.45; H, 3.12; N, 11.91. Found: C, 37.42; H, 3.13; N, 11.89. IR data (KBr, cm^{-1}): 3461(m), 1606(s), 1430(m), 1243(m), 1128(m), 1076(w), 879(w), 839(w), 696(m), 496(w).

2.1.4. Synthesis of $\{[\text{Mn}_6(\text{MIDC})_4(\text{py})_5(\text{H}_2\text{O})_4]\}_n$ (4**).** The procedure was the same as that for **3** except that CoCl_2 was replaced by MnCl_2 (0.10 mol L^{-3}). Upon cooling to room temperature, pale crystals were filtered and washed with ethanol. Yield: 56% (based on H_3MIDC). Elemental Anal. Calcd $\text{C}_{49}\text{H}_{45}\text{Mn}_6\text{N}_{13}\text{O}_{20}$ (1489.56): C, 38.67; H, 3.02; N, 12.22. Found: C, 38.69; H, 2.98; N, 12.19. IR data (KBr, cm^{-1}): 3417(w), 2919(w), 1564(s), 1424(s), 1251(m), 1123(m), 1036(w), 830(m), 687(m).

2.1.5. Synthesis of $\{[\text{Mn}_3(\text{MIDC})_2(\text{Phen})_3(\text{H}_2\text{O})_2]\}_n$ (5**).** The procedure was the same as that for **4** except that py (1 mL) was replaced by a solution of Phen (9.0 mg, 0.05 mmol) in 2 mL methanol. Upon cooling to room temperature, brown crystals were filtered and washed with ethanol. Yield: 43% (based on H_3MIDC). Elemental Anal. Calcd $\text{C}_{48}\text{H}_{36}\text{Mn}_3\text{N}_{10}\text{O}_{10}$ (1077.69): C, 53.45; H, 3.34; N, 12.99. Found: C, 53.48; H, 3.35; N, 12.97. IR data (KBr, cm^{-1}): 3473(w), 2919(w), 1574(s), 1419(s), 1352(m), 1243(m), 1114(m), 869(m), 830(m), 718(s), 633(w).

2.2. Crystal structure determination

The crystal structures were determined by single-crystal X-ray diffraction. Reflection data were collected on a Bruker SMART CCD area-detector diffractometer (Mo- $\text{K}\alpha$ radiation, graphite monochromator) at room temperature with ω -scan mode. Empirical adsorption corrections were applied to all data using SADABS. The structures were solved by direct methods and refined by full-matrix least squares on F^2 using SHELXTL 97 software [45]. Non-hydrogen atoms were refined anisotropically. All carbon-bound hydrogens were refined using a riding model. Hydrogens of water were located in difference Fourier maps and their positions were refined under an O–H bond-length restraint of 0.85 Å in **1–5**. All calculations were carried out using SHELXTL 97 [45] and PLATON [46]. The structure of **1** has large solvent-accessible voids, which contain a number of diffuse electron density peaks that could not be adequately identified. The SQUEEZE routine of PLATON was applied to the collected data, which resulted in significant reductions in R_1 and wR_2 [$I > 2\sigma$]. The corresponding R_1 and wR_2 : before SQUEEZE routine, 9.77 and 22.54% for **1**, after SQUEEZE routine, 5.44 and 15.02% for **1**. Chemical compositions of **1** were deduced from a combination of TGA and elemental analysis. The disordered 4,4'-bipy molecules in the 1-D channel of **2** were treated by performing split and occupancies refinement of the disordered atoms. For **5**, the disordered Phen coordinating to Mn1 was treated by performing split and occupancies refinement of the disordered atoms. The crystallographic data and pertinent information are given in table 1; selected bond lengths and angles are in table S1 (see online supplemental material at <http://dx.doi.org/10.1080/00958972.2015.1071483>).

Table 1. Crystal data and structure refinement for 1–5.

Compound	1	2	3	4	5
Empirical formula	C ₄₂ H ₃₀ N ₁₀ O ₈ Zn ₃	C ₅₂ H ₅₀ Co ₃ N ₁₂ O ₁₄	C ₂₂ H ₂₀ Co ₃ N ₆ O ₁₀	C ₄₈ H ₄₅ Mn ₆ N ₁₃ O ₂₀	C ₄₈ H ₃₆ Mn ₃ N ₁₀ O ₁₀
Formula weight	998.87	1243.83	705.23	1489.56	1077.69
Crystal system	Triclinic	Triclinic	Monoclinic	Monoclinic	Orthorhombic
Space group	<i>P</i> -1	<i>P</i> -1	<i>C</i> 2/ <i>c</i>	<i>P</i> 2 ₁ / <i>c</i>	<i>Pbcn</i>
<i>a</i> (Å)	11.6368(9)	11.525(2)	16.932(3)	16.815(3)	20.480
<i>b</i> (Å)	11.6437(9)	11.613(2)	10.254(2)	21.516(4)	19.861
<i>c</i> (Å)	11.8182(9)	11.769(2)	16.558(3)	20.888(7)	10.997
α (°)	79.3990(10)	65.61(3)	90	90	90
β (°)	64.7060(10)	79.25(3)	104.77(3)	128.120(18)	90
γ (°)	71.7480(10)	72.08(3)	90	90	90
Volume (Å ³)	1372.60(18)	1361.8(5)	2779.9(10)	5945(3)	4473.1
<i>Z</i>	1	1	4	4	4
ρ_{calc} (gcm ⁻³)	1.572	1.561	1.685	1.651	1.600
Absorption coeff. (mm ⁻¹)	1.382	0.980	1.833	1.719	0.908
θ range (°)	1.8–26.00	3.06–27.48	3.07–27.48	3.08–27.48	3.16–27.48
Reflections collected	7590	13,430	12,761	54,853	38,230
Completeness	98.5%	98.8%	99.6%	94.4%	97.4%
GOOF	1.085	1.109	1.063	1.050	1.049
<i>R</i> indexes [<i>I</i> > 2 σ (<i>I</i>)] ^a	0.0544	0.0496	0.0378	0.0879	0.0719
<i>wR</i> ₂ (all data) ^a	0.1577	0.1495	0.0941	0.2176	0.2092

$$^a R_1 = \Sigma ||F_o| - |F_c|| / \Sigma |F_o|; wR = [\Sigma w(F_o^2 - F_c^2)^2 / \Sigma w(F_o^2)]^{1/2}.$$

CCDC 980130, 980132, 980131, 980133, and 980134 for 1–5 containing the supplementary crystallographic data can be obtained free of charge from the Cambridge Crystallographic Data Center via http://www.ccdc.cam.ac.uk/data_request/cif.

3. Results and discussion

3.1. Crystal structures

3.1.1. Crystal structures of 1 and 2. Compounds 1 and 2 with different molecular formulas have the same crystal system, space group, and isostructural frameworks, so only the structure of 1 is described in detail as a representative example.

Three crystallographically independent Zn(II) ions in the asymmetric unit of 1 are all located at inversion centers [figure 1(a)]. Zn1 and Zn2 exhibit similar octahedral coordination environments, each of which is coordinated by two oxygens and two nitrogens from two symmetrical equivalent μ_3 -MIDC³⁻ anions, and two nitrogens from two 4,4'-bipy ligands. Zn3 is six-coordinate, binding to four carboxylate oxygens from two symmetrical equivalent μ_3 -MIDC³⁻ anions and two nitrogens from two 4,4'-bipy bridges. Zn–O/N bond distances around Zn range from 2.042(3) to 2.297(2) Å, and O/N–Zn–O/N bond angles range from 79.31(12)° to 180.0(2)°; the corresponding bond lengths and angles are listed in table S1.

Each MIDC³⁻ anion adopting bis-N,O-chelating mode connects six-coordinate Zn centers (Zn1 and Zn2) into a 1-D, metal–organic chain where Zn ions and MIDC³⁻ anions are almost coplanar. Then each MIDC³⁻ anion of 1-D chains adopting the bis-O,O-chelating

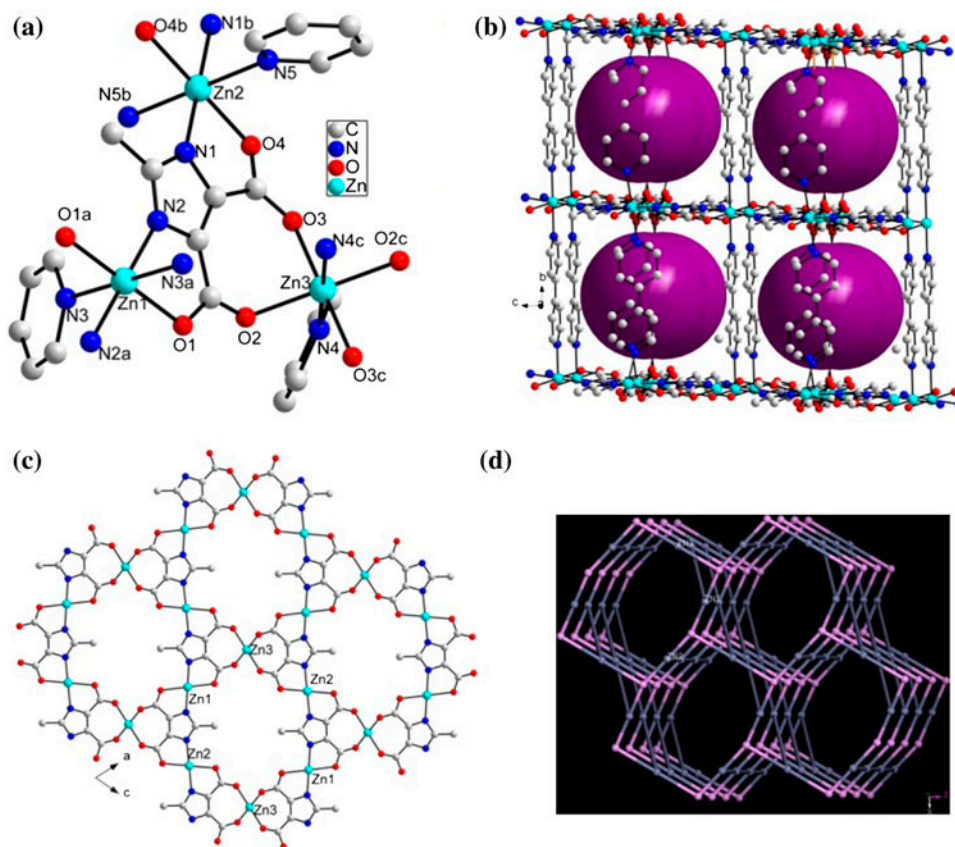


Figure 1. (a) Coordination environment of Zn^{II}, (b) [Zn₃(MIDC)₂]_n layer with 24-membered hexagonal rings, (c) 3-D network, (d) the topology with Schlafli symbol {10}{6.10²}₂{6⁴.8.10}₂ for 1.

mode joins Zn3 ions to generate a 2-D honeycomb-like layer of [Zn₃(MIDC)₂]_n with 24-membered hexagonal rings, which are constructed from six MIDC³⁻ anions, two Zn1, two Zn2, and two Zn3 [figure 1(b)]. Two types of pillared 4,4'-bipy bridges are found in 1. The two pyridine rings of the first type are coplanar while the two pyridine rings of the second type are twisted with a dihedral angle of 26.72°. The 2-D honeycomb-like layers in 1 are further pillared by two types of 4,4'-bipy molecules to give a 3-D coordination polymer with open hexagonal channels with the dimension of 11.64 × 12.55 Å (based on the distance of metal centers) along the *b* axis [figure 1(c)]. From another standpoint, there is a novel cage in 1 which is composed of four MIDC³⁻ anions, eight Zn ions, two coplanar 4,4'-bipy, and two noncoplanar 4,4'-bipy molecules. Then each cage links six symmetrically equivalent cages into a 3-D metal-organic framework [figure 1(c)]. Calculations performed using PLATON reveal a total solvent-accessible volume of 495.6 Å³ per unit cell, which counts for 36.1% of the cell volume [46], offering possibilities of gas adsorption and gas separation. From the perspective of network topology, MIDC³⁻ anions interacting with three Zn ions can be regarded as 3-connected nodes, and three crystallographically independent Zn ions can be all regarded as 4-connected nodes [figure 1(d)]. So the framework of 1

may be simplified into a 3-nodal net with Schläfli symbol $\{10\}\{6.10^2\}_2\{6^4.8.10\}_2$, as determined by TOPOS [47].

The isostructural frameworks of **1** and **2** are similar to recently reported complexes with the structural formula $\{M_3(\text{IDC})_2(4,4'\text{-bipy})_3\}_n$ ($M=\text{Co}$ or Zn) [38, 39], constructed by $M_3(\text{IDC})_2$ layers and $\mu_{2-4},4'$ -bipy bridges. The difference of the reported compounds and our compounds are the chosen organic ligands, which are IDC^{3-} in the reported compounds and MIDC^{3-} in our compounds. It should be noted that the methyl in the imidazole moiety of our compounds does not strongly affect the packing structures of **1** and **2**, they exhibit isostructural frameworks to the reported compounds. Though the unit cell volume of **2** is slightly smaller than that of **1**, calculations performed using PLATON reveal a total solvent-accessible volume (502.3 \AA^3) per unit cell, larger than that of **1** (495.6 \AA^3), correspondingly, the porosity of **2** is larger than that of **1**.

3.1.2. Crystal structure of 3. The asymmetric unit of **3** contains one and a half Co^{II} ion (Co1 and Co2), a μ_3 - MIDC^{3-} , a coordinated water and one pyridine molecule. Co2 is located on a twofold axis with occupancy of 0.5. As shown in figure 2(a), Co1 shows distorted trigonal bipyramidal geometry, which is defined by two nitrogens and two oxygens from two MIDC^{3-} anions and one oxygen from a coordinated water (O1w) with Co-O distances of $2.1034(19)$ – $2.1072(19) \text{ \AA}$ and Co-N distances of $2.002(3)$ – $2.023(2) \text{ \AA}$. Co2

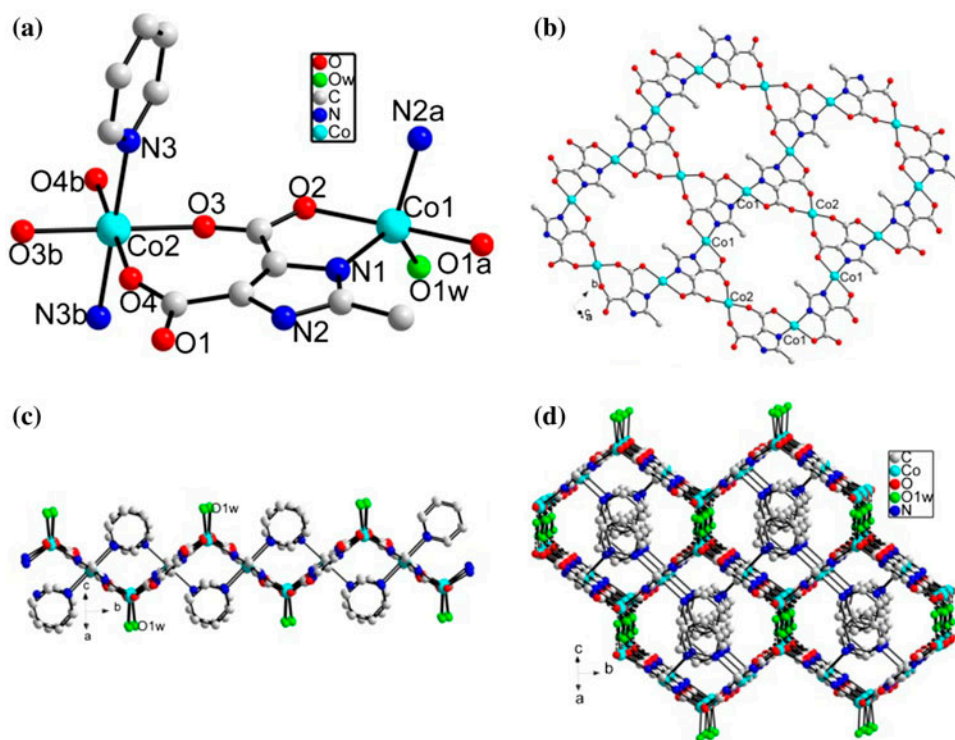


Figure 2. (a) Coordination environment of Co^{II} , (b) $[\text{Co}_3(\text{MIDC})_2]_n$ layer with 24-membered hexagonal rings, (c) the 2-D puckered layer, (d) the 3-D supramolecular network for **3**.

shows an octahedral geometry rather than trigonal bipyramidal geometry around Co1, which receives contributions from four carboxylate oxygens belonging to two symmetry equivalent μ_3 -MIDC³⁻ anions and two nitrogens belonging to two py ligands. The Co–N distance (2.177(3) Å) is slightly longer than Co–O distances (2.0376(17)–2.0633(18) Å); the corresponding bond lengths and angles are listed in table S1.

Each MIDC³⁻ connects five-coordinate Co1 ions into a wavelike 1-D zigzag chain in bis-N,O-chelating mode and then 1-D chains are connected by Co2 to generate a 2-D honeycomb-like layer of [Co₃(MIDC)₂]_n with 24-membered hexagonal rings [figure 2(b)]. Notably, MIDC³⁻ in **3** adopts identical coordination mode to that observed in **1** and **2**. However, the difference in **3** is represented by five-coordinate Co ions in place of six-coordinate metal centers in **1** and **2**. This feature has significant influence to the final structure of **3**, where the layers are arranged in a wavelike fashion, in contrast to the flat architecture in **1** and **2**.

Furthermore, the final crystal structure of **3** is thoroughly different from those of **1** and **2** because the μ_{2-4} ,4'-bipy bridges were replaced by the terminal py ligands. As shown in figure 2, py molecules lie on two sides of the 2-D wavelike layers in an anti-parallel fashion. At the wave crest and trough of the 2-D wavelike layer, the coordinated waters (O1w) outstretch and act as hydrogen donors [figure 2(c)] to interact with O5 and O6 of carboxyl groups of MIDC³⁻ from a neighboring layer as hydrogen acceptor through O–H···O hydrogen bonds with O···O distances of 3.1 Å [figure 2(d)].

Compared with recently reported [Zn₃(MIDC)₂(H₂O)₂(DMF)₂]_n [41], both of them contain the similar metal coordination geometry and coordination modes of organic linkers, however, the different terminal ligands and metal centers result in different wavelike frameworks (rigid py molecules and Co ions for **3**; flexible DMF molecules and Zn ions for [Zn₃(MIDC)₂(H₂O)₂(DMF)₂]_n). Moreover, rigid py molecules result in coplanar arrangement of six-coordinate Co centers and two MIDC³⁻ anions in **3**, however, flexible DMF molecules result in the two MIDC³⁻ anions coordinating to the same six-coordinate Zn centers which are not coplanar but parallel to each other (figure S1).

3.1.3. Crystal structure of 4. X-ray crystallographic analysis reveals that **4** is a 2-D wavelike layer based on [Mn₃(MIDC)₂]_n and crystallizes in the space group *P2₁/c*. The asymmetric unit of **4** contains six crystallographically independent Mn(II) ions, four μ_3 -MIDC³⁻ anions, four coordinated waters, and five coordinated py molecules [figure 3(a)]. Mn1, Mn2, and Mn6 exhibit similar trigonal bipyramidal coordination environments, each of which is bound to two oxygens and two nitrogens from two independent μ_3 -MIDC³⁻ anions, and one oxygen from a water. Mn3 and Mn5 exhibit octahedral geometries, each coordinated by four carboxylate oxygens from two independent μ_3 -MIDC³⁻ anions and two nitrogens from two py terminal ligands. Mn4 is six-coordinate with two nitrogens and two oxygens from two MIDC³⁻ anions, and one oxygen from a water molecule, and one nitrogen atom from a py molecule, forming a distorted octahedral geometry. The Mn–O/N bond distances around Mn centers are 2.087(6)–2.353(9) Å and the O/N–Mn–O/N bond angles 75.2(2)–178.4(2)°; the corresponding bond lengths and angles are listed in table S1.

MIDC³⁻ anions connect five- (Mn1, Mn2, Mn6) and six-coordinate Mn centers (Mn4) into a 1-D wavelike zigzag chain in bis-N,O-chelating mode. However, the wavelike zigzag chain in **4** is different from that of **3**. The repeating unit of the 1-D chain in **3** is comprised of one metal and one MIDC³⁻, however, the repeating unit of the 1-D chain in **4** is

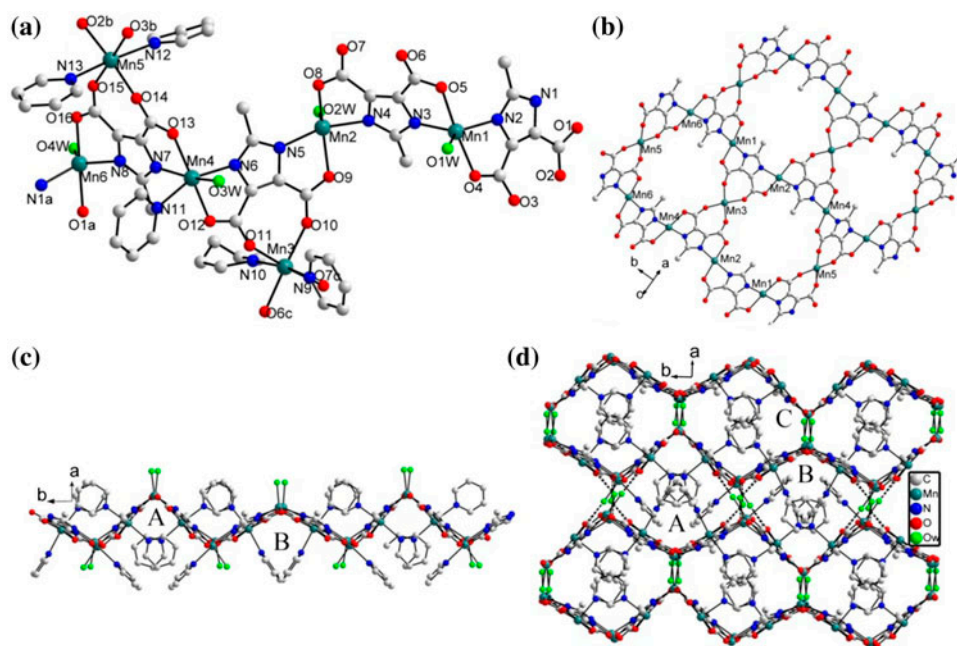


Figure 3. (a) Coordination environment of Mn^{II} , (b) $[\text{Mn}_3(\text{MIDC})_2]_n$ layer with 24-membered hexagonal rings, (c) the 2-D puckered layer with two crests and troughs (A and B), (d) the 3-D supramolecular network with three kinds of channels (A–C) for 4.

composed of two metal ions and two independent MIDC^{3-} ligands. Thus, the wavelike zigzag chain in **3** contains a crest and a trough during each period; however, the chain in **4** contains two crests and troughs during each period.

Mn1 and Mn4 are located at two troughs, whereas Mn2 and Mn6 are located at the two crests. The neighboring Mn–Mn distances are 3.0–3.1 Å. The period of the chain is about 21.5160 Å. To the best of our knowledge, the wavelike chain containing two crests and troughs during each period was not reported previously. 1-D chains are connected by Mn3 and Mn5 ions to generate a 2-D wavelike layer of $[\text{Mn}_3(\text{MIDC})_2]_n$ with two crests and troughs during each period. Coordinated py molecules were decorated on two sides of the 2-D wavelike layer. At the wave crest and trough of the 2-D wavelike layer, O1w , O2w , O3w , and O4w outstretch just like the water molecules in **3**; there also exist strong $\text{O-H}\cdots\text{O}$ hydrogen bonds with these water molecules as hydrogen donors and carboxylate oxygens from neighboring wavelike layer. Therefore, 2-D layers are joined by these hydrogen contacts into a 3-D supramolecular structure.

There are three types of 1-D hexagonal channels (Channel A, B, and C) in the 3-D supramolecular network of **4** along the c axis. Channels A and B both possessing the same shapes and dimensions are alternately arranged in an anti-parallel fashion along the b axis and Channel C with dimension of $10.35 \times 10.54 \text{ \AA}^2$ exists in packing layers via hydrogen bonds between water molecules and carboxylate oxygens [figure 3(d)]. All these channels are filled by coordinated py molecules.

A comparison of **3** and **4** shows that the main difference is in the coordination environment of metal centers, only five-coordinate Co ions were involved in formation of the 1-D

zigzag chain in **3**, while both five- and six-coordinate Mn ions were found in the 1-D chain of **4**. Clearly the different wavelike layers of **3** and **4** are dictated by the coordination geometry of metal centers.

Comparing $[\text{Mn}_6(\text{MIDC})_4(\text{py})_5(\text{H}_2\text{O})_4]$ (**4**) and the recently reported $[\text{Mn}_6(\text{EIDC})_4(\text{py})_4(\text{H}_2\text{O})_4]$ [32], both consist of Mn centers, similar imidazole dicarboxylate, coordinated py, and water molecules, but differ for the number of coordinated py molecules. Different coordination environments of Mn centers are observed in the two compounds: there are three five- and three six-coordinate Mn ions in the asymmetric unit of **4**; four five- and two six-coordinate Mn centers in $[\text{Mn}_6(\text{EIDC})_4(\text{py})_4(\text{H}_2\text{O})_4]$. These features result in a different puckered layer, which shows two crests and troughs during each period in **4**, while containing a crest and a trough during each period in $[\text{Mn}_6(\text{EIDC})_4(\text{py})_4(\text{H}_2\text{O})_4]$.

3.1.4. Crystal structures of 5. When chelating Phen was introduced into the reaction system, single crystals of **5** were obtained. The asymmetric unit of **5** contains two crystallographically independent Mn(II) ions, one μ_3 -MIDC³⁻ anion, 1.5 Phen molecules, and one lattice Phen [figure 4(a)]. Mn1 is located on a twofold axis and has octahedral geometry with four carboxylate oxygens from two symmetry equivalent μ_3 -MIDC³⁻ anions and two nitrogens from a Phen. Around Mn1, three *trans* angles are not less than 156° and the *cis* angles are 85.1(2)–102.7(3)°, indicating distortion of the Mn1 octahedral geometry. Two MIDC³⁻ anions and one Phen chelate Mn1 in O,O- and N,N-chelating modes, forming a chiral manganese complex with right-handed screw (Δ) configuration. Mn2 is bonded to

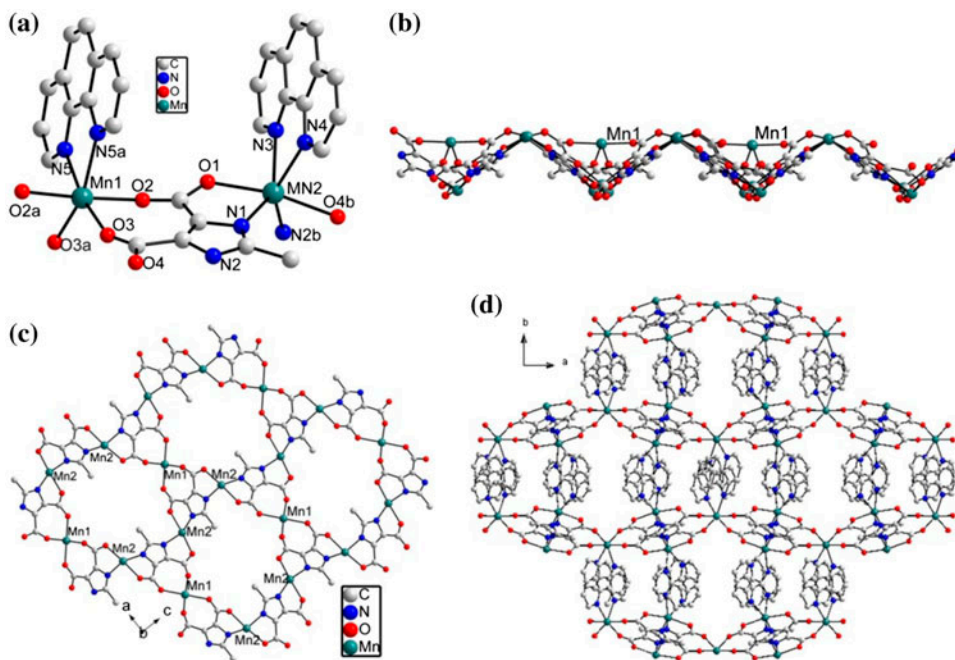


Figure 4. (a) Coordination environment of Mn^{II} , (b) the 2-D abnormal puckered layer (Phen molecules are omitted for clarity), (c) $[\text{Mn}_3(\text{MIDC})_2]_n$ layer with 24-membered hexagonal rings, (d) the 3-D supramolecular network for **5**. Hydrogens are omitted.

two nitrogens and two oxygens from two symmetry equivalent MIDC³⁻ anions and two nitrogens from one Phen. Mn2 is chelated by two neighboring MIDC³⁻ anions and one Phen ligand in O,N- and N,N-chelating modes, leading to metal-centered chirality with left-handed screw (Λ) configuration [48]. The dihedral angle of the two planes of the two MIDC³⁻ belonging to one manganese complex is 112.544°. All Mn–N/O bond lengths are comparable to the reported imidazole dicarboxylate-based Mn complexes [32, 41]. One five-membered (N5-C23-C23a-N5a-Mn1) and two seven-membered rings (O2-C4-C1-C2-C5-O3-Mn1) were formed through Mn1 and coordinated ligands, however, three five-membered rings (O1-C4-C1-N1-Mn2, O4-C5-C2-N2-Mn2, and N3-C18-C17-N4-Mn2) are formed around Mn2 and coordinated ligands.

Each MIDC³⁻ connects six-coordinate Mn2 ions into a 1-D wavelike chain in bis-N,O-chelating mode. 1-D chains are connected by Mn1 to generate a 2-D abnormal layer of [Mn₃(MIDC)₂]_n with 24-membered hexagonal rings [figure 4(b) and (c)].

The introduction of chelating Phen ligands influences the structure of **5**: MIDC³⁻ ligands have been effectively controlled to the tri(chelating) coordination mode, and the introduced Phen ligands also chelate. Therefore, the manganese ions in **5** are coordinated by three chelates, resulting in the formation of the first puckered [M₃(L)₂]_n layer structure decorated by chelating neutral ligands (L = imidazole-4,5-dicarboxylic acid or its analog). To the best of our knowledge, several compounds like [Mn₆(EIDC)₄(py)₄(H₂O)₄]_n [32], [Zn₃(MIDC)₂(H₂O)₂(DMF)₂]_n [41], **3**, and **4** contain [M₃(L)₂]_n wavelike layers, all of which are based on both five- and six-coordinate metal centers, however, the wavelike [M₃(L)₂]_n layer in **5** was the first example which is based only on six-coordinate metal centers.

Strong $\pi \cdots \pi$ interactions exist among Phen molecules from two neighboring [Mn₃(MIDC)₂]_n layers, and the 2-D layers were interdigitated into a 3-D supramolecular network via these interactions [figures 4(d) and S2].

3.1.5. Discussion. Control of coordination modes of chosen organic ligands is usually difficult. Coordination polymers **1–5** were prepared through reactions of H₃MIDC, neutral terminal or bridging ligands, metal ions, and NH₂NH₂·H₂O under hydrothermal conditions. We have developed a new method to control the special coordination mode of MIDC³⁻ ligands using hydrazine as the deprotonating agent and spontaneously controlling the pH of reaction mixture above six, which was effective for control of tri(chelating) coordination of MIDC³⁻. We also attempt to use triethylamine or NaOH to take the place of hydrazine, and those attempts are not successful [41]. Though the explicit control mechanism is still unknown, successful syntheses of **1–5** demonstrate that this method is very effective.

The coordination mode of EIDC³⁻ can also be effectively controlled under the help of hydrazine but did not give the stable layer of [M₃(EIDC)₂]_n in {Co₃(EIDC)₂(H₂O)₅}_n and {Zn₃(EIDC)₂(H₂O)₄}_n reported [43], when there are no neutral terminal or bridging ligands involved in the reactions. So, it is possible that hydrazine is helpful to the formation of MIDC³⁻ or EIDC³⁻ anions with tri(chelating) coordination modes but neutral terminal or bridging ligands benefit the stabilities of [M₃(L)₂]_n layers (L = MIDC or EIDC).

In **1–5**, each MIDC³⁻ links three metal ions in the same tri(chelating) coordination mode, however, the chelates formed by metal ions and MIDC³⁻ anions show differences. Though each MIDC³⁻ links three six-coordinate metal ions in **1**, **2**, and **5**, MIDC³⁻ anions in bis-N, O and O,O-chelating modes occupy the four positions of the equatorial plane of six-coordinate metal centers in **1** and **2**, resulting in the dihedral angle between two MIDC³⁻ anions coordinating to the same metal ion of 180°. MIDC³⁻ anions occupy some sites of

both the axial and equatorial plane positions due to chelating Phen, and the corresponding dihedral angle is 112.544° , leading to the formation of 2-D wavelike layer in **5**, different than the coplanar layer of **1** and **2**.

Each MIDC^{3-} links two five-coordinate and one six-coordinate Co ions in **3**, however, there exist two kinds of chelates formed by metal ions and MIDC^{3-} anions in **4**. One is formed by MIDC^{3-} anion chelating two five- and one six-coordinate Mn ions and the other is formed by MIDC^{3-} anion linking one five-coordinate and two six-coordinate Mn ions. In **1–4**, MIDC^{3-} anions using O,O-chelating modes occupy four positions of the equatorial plane of six-coordinate metal centers joining 1-D chains into a 2-D layer, however, MIDC^{3-} anions simultaneously occupy axial and equatorial positions of Mn1 in **5**. In summary, tri (chelating) coordination of MIDC^{3-} anions is effectively controlled, however, the chelates formed by metal ions and MIDC^{3-} anions are different.

Coordination of H_3MIDC was effectively controlled and induced the formation of the stable $[\text{M}_3(\text{MIDC})_2]_n$ layers, which will be helpful for the rational synthesis of the targeted complexes based on imidazole dicarboxylate.

3.2. TG curves of 1–5

The thermal behaviors of **1–5** were studied from 14 to 700°C under air. The TGA plots (figure 5) reveal that **1** and **2** decompose through three major processes. The first loss of **1** and **2** correspond to loss of lattice water (obsd: 13.18% for **1**, 9.95% for **2**; calcd. 11.09% for **1**, 8.69% for **2**). The second weight loss of **1** and **2** was characteristic of the combustion of MIDC^{3-} (obsd: 23.49% for **1**, 27.08% for **2**). The third weight loss of **1** and **2** mainly correspond to combustion of 4,4'-bipy (obsd: 44.48% for **1**, 43.41% for **2**). The total weight loss of **1** and **2** amounted to 81.75 and 81.27%, respectively. The remaining weights for **1** and **2** correspond to the formation of ZnO and CoO, respectively (obsd. 18.25% for **1**; 18.23% for **2**; calcd. 18.78% for **1**, 18.08% for **2**). However, **3–5** decomposed through two major processes. The first weight loss of **3** was attributed to the loss of coordinated water and py from $30\text{--}260^\circ\text{C}$ (obsd: 27.78% for **3**; calcd. 27.51% for **3**). The second weight loss of **3** was characteristic of the combustion of MIDC^{3-} . The total weight loss of **3** amounted to 68.25%. The remaining weights for **3** correspond to CoO (obsd. 31.75% for **3**; calcd.

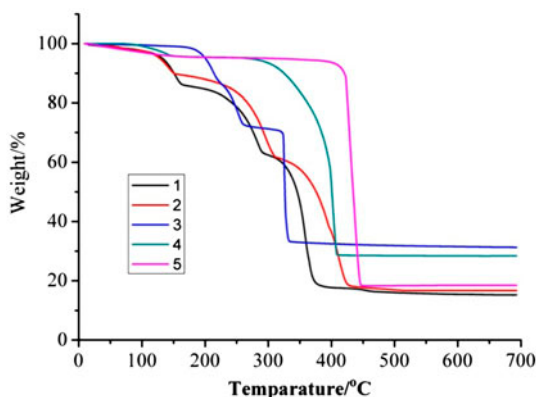


Figure 5. The TGA curves of **1–5**.

31.48% for **3**). The first weight losses of **4** and **5** correspond to the loss of coordinated water below 160 °C (obsd: 4.45% for **4**, 4.24% for **5**; calcd. 4.83% for **4**, 3.34% for **5**). The second weight loss of **4** and **5** was due to the combustion of organic ligands (obsd: 66.97% for **4**, 77.40% for **5**). The total weight loss of **4** and **5** amounted to 71.44 and 81.64%, respectively. The remaining weights for **4** and **5** both correspond to the formation of MnO (obsd. 28.56% for **4**, 18.36% for **5**; calcd. 28.60% for **4**, 19.76% for **5**).

3.3. PL spectrum of **1**

The photoluminescence spectra of H₃MIDC, 4,4'-bipy, and **1** in the solid state at room temperature are shown in figure 6. The photoluminescence spectra of H₃MIDC and 4,4'-bipy reveal intense fluorescent emissions at 425 nm ($\lambda_{\text{ex}} = 254$ nm) for H₃MIDC and 419 nm for 4,4'-bipy ($\lambda_{\text{ex}} = 340$ nm). Similarly, **1** also exhibits blue photoluminescence with emission maxima at 467 nm upon excitation at 254 nm. Compared with the PL spectra of organic ligands, the emission bands for **1** are similar to that found for free H₃MIDC in terms of position and band shape. Therefore, the emission bands of **1** are mainly due to an intraligand emission similar with the reported d¹⁰ metal complexes with N-donor carboxylate ligands [28, 38]. Therefore, the emissions of **1** may be assigned to $\pi^* \rightarrow \pi$ or $\pi^* \rightarrow n$ transition of H₃MIDC ligands.

3.4. Magnetic properties of **2–5**

Variable-temperature magnetic susceptibilities for **2–5** were measured in the temperature range of 2–300 K under a 1000 Oe applied field. The $\chi_{\text{m}}T$ per Co(II) ion *versus* T curves are shown in figure 7, the $\chi_{\text{m}}T$ values at 300 K for **2** and **3** are 1.94 and 2.28 cm³ K mol⁻¹, respectively, which are higher than the spin-only value of 1.875 cm³ K mol⁻¹ for Co^{II} (Co^{II}, $S = 3/2$ and $g = 2.0$), indicating the spin-orbit coupling contribution of high-spin Co^{II}. The $\chi_{\text{m}}T$ curves decrease continuously with decreasing temperature and reach a minimum at 6.9 K (0.46 cm³ K mol⁻¹ for **2**, 0.55 cm³ K mol⁻¹ for **3**) and then increase to a maximum value (0.51 cm³ K mol⁻¹ at 5.48 K for **2**, 0.60 cm³ K mol⁻¹ at 4.96 K for **3**). Further cooling, $\chi_{\text{m}}T$ values drops sharply at 2 K (0.015 cm³ K mol⁻¹ for **2**, 0.30 cm³ K mol⁻¹ for **3**). The increase in the $\chi_{\text{m}}T$ at low temperatures is probably due to spin-canting behaviors [49,

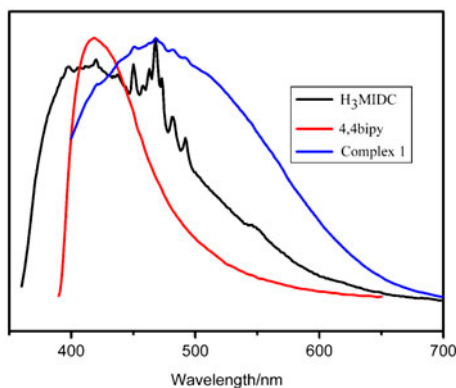


Figure 6. Solid-state emission spectra for **1**, H₃MIDC and 4,4-bipy at room temperature.

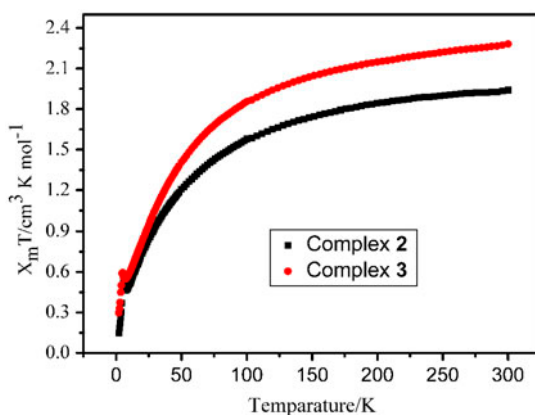


Figure 7. Plots of $\chi_m T$ vs. T for **2** and **3**.

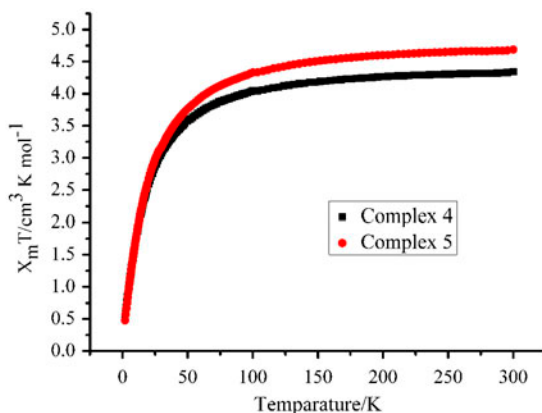


Figure 8. Plots of $\chi_m T$ vs. T for **4** and **5**.

50]. In χ_m^{-1} versus T curve, the magnetic susceptibility data follow the Curie–Weiss law ($\chi_m = C/(T-\theta)$) above 20 K with Curie constant $C = 2.15 \text{ cm}^3 \text{ K mol}^{-1}$ and the Weiss constant $\theta = -33.24 \text{ K}$ for **2**, and $C = 2.58 \text{ cm}^3 \text{ K mol}^{-1}$ and $\theta = -40.13 \text{ K}$ for **3**. According to the formulas $C = 0.125 g^2 \Sigma S(S+1)$, the g value is 2.14 and 2.35 for **2** and **3**, respectively. The larger negative value of θ and the decrease in $\chi_m T$ indicates strong antiferromagnetic interactions between Co (II) centers in **2** and **3** [39, 51].

As shown in figure 8, the $\chi_m T$ value of per Mn^{II} ion for **4** and **5** at 300 K is 4.34 and $4.69 \text{ cm}^3 \text{ K mol}^{-1}$, respectively, which are close to the expected value ($4.38 \text{ cm}^3 \text{ K mol}^{-1}$) for magnetically non-interacting Mn^{II} ions with $S = 5/2$ and $g = 2.0$. The $\chi_m T$ values for **4** and **5** decrease continuously with decreasing temperature and reach a minimum at 2 K ($0.51 \text{ cm}^3 \text{ K mol}^{-1}$ for **4**, $0.48 \text{ cm}^3 \text{ K mol}^{-1}$ for **5**). In the χ_m^{-1} versus T curve, the magnetic susceptibility data follow the Curie–Weiss law ($\chi_m = C/(T-\theta)$) in the temperature range 2–300 K with a Curie constant $C = 4.48 \text{ cm}^3 \text{ K mol}^{-1}$ and the Weiss constant $\theta = -10.79 \text{ K}$ for **4**, and $C = 4.83 \text{ cm}^3 \text{ K mol}^{-1}$, and $\theta = -10.13 \text{ K}$ for **5**. According to the formulas

$C = 0.125 g^2 \Sigma S(S + 1)$, the g value is 2.02 and 2.10 for **4** and **5**, respectively. The negative value of θ and the decrease in $\chi_m T$ indicates weak antiferromagnetic interactions between Mn^{II} centers in **4** and **5** [32].

4. Conclusion

Five metal imidazole dicarboxylate complexes have been synthesized under hydrothermal conditions and fully characterized by elemental analyses, IR spectroscopy, single-crystal X-ray diffraction, and thermogravimetric analysis. The results revealed that hydrazine can effectively control the coordination modes of H_3MIDC and gave a series of new coordination compounds containing honeycomb-like $[M_3(MIDC)_2]_n$ layers neutral terminal or bridging ligands. Control of the stable $[M_3(MIDC)_2]_n$ layer will be helpful for rational synthesis of the targeted complexes based on imidazole dicarboxylate; further research for the construction of new architectures with imidazole dicarboxylate is underway in our laboratory.

Supplementary material

Bond lengths and bond angles of **1-5** and additional figure S1.

Disclosure statement

No potential conflict of interest was reported by the authors.

Funding

This work was supported by the National Natural Science Foundation of China [grant number 21201155]; Natural Science Young Scholars Foundation of Shanxi Province [grant numbers 2012021007-5 and 2013021008-6]; Program for the Top Young Academic Leaders of Higher Learning Institutions of Shanxi.

References

- [1] A. Bétard, R.A. Fischer. *Chem. Rev.*, **112**, 1055 (2012).
- [2] K. Binnemans. *Chem. Rev.*, **109**, 4283 (2009).
- [3] R. Chakrabarty, P.S. Mukherjee, P.J. Stang. *Chem. Rev.*, **111**, 6810 (2011).
- [4] Y. Cui, Y. Yue, G. Qian, B. Chen. *Chem. Rev.*, **112**, 1126 (2012).
- [5] L.E. Kreno, K. Leong, O.K. Farha, M. Allendorf, R.P. Van Duyne, J.T. Hupp. *Chem. Rev.*, **112**, 1105 (2012).
- [6] M. O’Keeffe, O.M. Yaghi. *Chem. Rev.*, **112**, 675 (2012).
- [7] N. Stock, S. Biswas. *Chem. Rev.*, **112**, 933 (2012).
- [8] M.P. Suh, H.J. Park, T.K. Prasad, D.W. Lim. *Chem. Rev.*, **112**, 782 (2012).
- [9] W. Zhang, R.G. Xiong. *Chem. Rev.*, **112**, 1163 (2012).
- [10] M. Nakano, H. Oshio. *Chem. Soc. Rev.*, **40**, 3239 (2011).
- [11] M. O’Keeffe. *Chem. Soc. Rev.*, **38**, 1215 (2009).
- [12] O. Shekhah, J. Liu, R.A. Fischer, C. Wöll. *Chem. Soc. Rev.*, **40**, 1081 (2011).
- [13] X.Y. Wang, C. Avendaño, K.R. Dunbar. *Chem. Soc. Rev.*, **40**, 3213 (2011).
- [14] A.U. Czaja, N. Trukhan, U. Müller. *Chem. Soc. Rev.*, **38**, 1284 (2009).
- [15] L.J. Murray, M. Dincă, J.R. Long. *Chem. Soc. Rev.*, **38**, 1294 (2009).
- [16] T. Uemura, N. Yanai, S. Kitagawa. *Chem. Soc. Rev.*, **38**, 1228 (2009).
- [17] M.D. Allendorf, C.A. Bauer, R.K. Bhakta, R.J.T. Houk. *Chem. Soc. Rev.*, **38**, 1330 (2009).

- [18] G. Férey, C. Serre. *Chem. Soc. Rev.*, **38**, 1380 (2009).
- [19] W. Lu, Z. Wei, Z.Y. Gu, T.F. Liu, J. Park, J. Park, J. Tian, M. Zhang, Q. Zhang, T. Gentle III, M. Bosch, H.C. Zhou. *Chem. Soc. Rev.*, **43**, 5561 (2014).
- [20] V. Stavila, A.A. Talin, M.D. Allendorf. *Chem. Soc. Rev.*, **43**, 5994 (2014).
- [21] L.Q. Mo, J.H. Jia, L.J. Sun, Q.M. Wang. *Chem. Commun.*, **48**, 8691 (2012).
- [22] Y.Y. Yin, X.Y. Chen, X.C. Cao, W. Shi, P. Cheng. *Chem. Commun.*, **48**, 705 (2012).
- [23] S.C. Chen, Z.H. Zhang, K.L. Huang, Q. Chen, M.Y. He, A.J. Cui, C. Li, Q. Liu, M. Du. *Cryst. Growth Des.*, **8**, 3437 (2008).
- [24] F. Gándara, M.E. Medina, N. Snejko, E. Gutiérrez-Puebla, D.M. Proserpio, M.A. Angeles Monge. *CrystEngComm.*, **12**, 711 (2010).
- [25] B.R. Manzano, F.A. Jalón, M.L. Soriano, M.C. Carrión, M.P. Carranza, K. Mereiter, A.M. Rodríguez, A. de la Hoz, A. Sánchez-Migallón. *Inorg. Chem.*, **47**, 8957 (2008).
- [26] J.J. Zhang, L. Wojtas, R.W. Larsen, M. Eddaoudi, M.J. Zaworotko. *J. Am. Chem. Soc.*, **131**, 17040 (2009).
- [27] N. Stock, S. Biswas. *Chem. Rev.*, **112**, 933 (2011).
- [28] Q.G. Zhai, R.R. Zeng, S.N. Li, Y.C. Jiang, M.C. Hu. *CrystEngComm.*, **15**, 965 (2011).
- [29] S. Wang, T.T. Zhao, G.H. Li, L. Wojtas, Q.S. Huo, M. Eddaoudi, Y.L. Liu. *J. Am. Chem. Soc.*, **132**, 18038 (2012).
- [30] C.J. Wang, T. Wang, W. Zhang, H.J. Lu, G. Li. *Cryst. Growth Des.*, **12**, 1091 (2012).
- [31] Z.F. Li, X.B. Luo, Y.C. Gao, H.J. Lu, G. Li. *Inorg. Chim. Acta.*, **384**, 352 (2012).
- [32] F. Zhang, Z. Li, T. Ge, H. Yao, G. Li, H. Lu, Y. Zhu. *Inorg. Chem.*, **49**, 3776 (2010).
- [33] Y.G. Sun, M.Y. Guo, G. Xiong, F. Ding, L. Wang, B. Jiang, M.C. Zhu, E.J. Gao, F. Verpoort. *J. Coord. Chem.*, **63**, 4188 (2010).
- [34] F.-J. Yin, H. Zhao, X.-Y. Xu, M. Guo. *J. Coord. Chem.*, **66**, 3199 (2013).
- [35] M.H. Alkordi, J.A. Brant, L. Wojtas, V.C. Kravtsov, A.J. Cairns, M. Eddaoudi. *J. Am. Chem. Soc.*, **131**, 17753 (2009).
- [36] M.H. Alkordi, Y. Liu, R.W. Larsen, J.F. Eubank, M. Eddaoudi. *J. Am. Chem. Soc.*, **130**, 12639 (2008).
- [37] R.Q. Zou, H. Sakurai, Q. Xu. *Angew. Chem. Int. Ed. Engl.*, **45**, 2542 (2006).
- [38] W.G. Lu, L. Jiang, X.L. Feng, T.B. Lu. *Cryst. Growth Des.*, **6**, 564 (2006).
- [39] Y.L. Wang, D.Q. Yuan, W.H. Bi, X. Li, X.J. Li, F. Li, R. Cao. *Cryst. Growth Des.*, **5**, 1849 (2005).
- [40] C.J. Li, S. Hu, W. Li, C.K. Lam, Y.Z. Zheng, M.L. Tong. *Eur. J. Inorg. Chem.*, **2006**, 1931 (2006).
- [41] J.F. Song, R.S. Zhou, T.P. Hu, Z.O. Chen, B.B. Wang. *J. Coord. Chem.*, **63**, 4201 (2010).
- [42] R.S. Zhou, J.F. Song, Y.B. Li, C.Y. Xu, X.F. Yang. *Z. Anorg. Allg. Chem.*, **637**, 251 (2011).
- [43] L. Sun, J.F. Song, R.S. Zhou, J. Zhang, L. Wang, K.L. Cui, X.Y. Xu. *J. Coord. Chem.*, **67**, 822 (2014).
- [44] G. Tsukamoto, K. Yoshino, T. Kohno, H. Ohtaka, H. Kagaya, K. Ito. *J. Med. Chem.*, **23**, 734 (1980).
- [45] G.M. Sheldrick. *SHELXS 97, Program for Crystal Structure Refinement*, University of Göttingen, Göttingen (1998).
- [46] A.L. Spek. *Molecular Geometry Program*, University of Utrecht, The Netherlands (1999).
- [47] V.A. Blatov, A.P. Shevchenko, V.N. Serezhkin. *J. Appl. Cryst.*, **33**, 1193 (2000).
- [48] J.J. Jodry, R. Frantz, J. Lacour. *Inorg. Chem.*, **43**, 3329 (2004).
- [49] H.H. Ko, J.H. Lim, H.C. Kim, C.S. Hong. *Inorg. Chem.*, **45**, 8847 (2006).
- [50] X.Y. Wang, L. Wang, Z.M. Wang, G. Su, S. Gao. *Chem. Mater.*, **17**, 6369 (2005).
- [51] Y.F. Bi, X.T. Wang, W.P. Liao, X.F. Wang, X.W. Wang, H.J. Zhang, S. Gao. *J. Am. Chem. Soc.*, **131**, 11650 (2009).